



Doubly-heavy tetraquark at finite temperature in a holographic model

Xi Guo, Jia-Jie Jiang, Xuan Liu, Xun Chen^a, Dong Xiang^b, Xiao-Hua Li^c

School of Nuclear Science and Technology, University of South China, Hengyang 421001, China

Received: 15 September 2023 / Accepted: 16 January 2024 / Published online: 30 January 2024
© The Author(s) 2024

Abstract In this paper, we employ gauge/gravity duality to investigate the string breaking and melting of doubly-heavy tetraquark that includes two heavy quarks and two light antiquarks in a holographic model at finite temperature. Firstly, four different configurations of $QQ\bar{q}\bar{q}$ are studied at different separation distances of the heavy quarks at finite temperatures. At high temperature, $QQ\bar{q}\bar{q}$ will melt at certain distances and the screening distance has been given for different temperatures. As the temperature continues to increase, some configurations of doubly-heavy tetraquark can not exist. Furthermore, we investigate three decay modes of $QQ\bar{q}\bar{q}$ and compare the potential energy of $QQ\bar{q}\bar{q}$ with that of QQq at finite temperature.

1 Introduction

The gauge/gravity duality has been widely recognized as a fundamental feature of quantum gravity, and extensive research has been carried out in this field over the past two decades, leading to many important findings [1]. Holographic QCD offers a novel approach to study and compute the properties of various physical phenomena in QCD. Studying heavy quarkonium is beneficial for understanding the properties of quark–gluon plasma (QGP), as well as validate our understanding of the interactions between hadrons and fundamental particles [2, 3]. In holographic QCD, we can study the interaction between quarks and antiquarks by placing a pair of them inside a bulk. Then, we can utilize the tools of string theory to calculate the interaction between the two quarks and their corresponding potential energy.

The string breaking phenomenon is a result of the nonperturbative effects of QCD. Up to now, lattice QCD has been

effectively utilized to investigate this phenomenon, albeit limited to meson modes at zero temperature and zero chemical potential [4]. As is widely acknowledged, the environment in which tetraquark are situated can often be complex. Therefore, introducing high-temperature factors into the model to study the behavior of four quark potentials at elevated temperatures can aid in better understanding the behavior of tetraquark under extreme conditions. In previous studies, it has been discovered that under sufficiently high temperatures, thermal excitations produce a plasma of quarks and gluons [5]. Subsequently, they discussed the potential at finite temperatures [5–7]. The deformed AdS_5 model [8–10] and Einstein–Maxwell–Dilaton model are employed to compute the quark–antiquark potential [11–28] in these researches.

Recently, at the Large Hadron Collider, the LHCb collaboration observed a hadron state that contains four quarks [29, 30]. This tetraquark contains two charm quarks, a \bar{u} and a \bar{d} quark, with a mass of about $3875 \text{ MeV}/c^2$. This finding has renewed interest in studying the tetraquark theory. It is worth noting that lattice gauge theory is still a fundamental tool for studying non-perturbative phenomena in QCD, but research results on the potential of $QQ\bar{q}\bar{q}$ are limited [31–36].

The tetraquark model used in this paper was proposed by Andreev [37]. This model assumes that the heavy quarks are significantly heavier than the typical energy scale of the system, allowing us to treat them as static. The interaction potential between the quarks is determined by their relative separation. The main reason for studying this model is that its results on both quark–antiquark and tetraquark potentials are consistent with lattice calculations and QCD phenomenology [4, 38]. At zero temperature, the timelike Wilson loop is realized by a U-shaped macroscopic string for any interquark separation. At finite temperature, we have seen that the string configuration is either a pair of straight strings or U-shaped [5]. Our technique for extracting the potential of $QQ\bar{q}\bar{q}$ is similar to the one used in lattice QCD. We extract the poten-

^a e-mail: chenxunhep@qq.com (corresponding author)

^b e-mail: xiangdong@usc.edu.cn (corresponding author)

^c e-mail: lixiaohuaphysics@126.com (corresponding author)

tial from the expectation value of the $QQ\bar{q}\bar{q}$ Wilson loop, $W_{QQ\bar{q}\bar{q}}(R, T)$. The $QQ\bar{q}\bar{q}$ Wilson loop consists of heavy quark paths and light quark propagators. The separation distance between heavy quark pairs and the potential energy relationship of the model were calculated and analyzed at finite temperature [39–47]. Subsequently, three decay modes of tetraquark were studied to determine the most probable decay mode that occurs at high temperatures and to compare it with the decay of three quarks.

Section 2 provides a brief review of the theoretical foundation of the model and establishes a framework for studying $QQ\bar{q}\bar{q}$ at finite temperature. Section 3 involves numerical solutions for the energy and separation distance between heavy quarks for these configurations at different temperatures. This is followed by a discussion of the results in Sect. 4. In this section, we will also discuss the melting of $QQ\bar{q}\bar{q}$ strings at finite temperatures by analyzing potential energy trends. Later in Sect. 5, the three types of decay modes in the $QQ\bar{q}\bar{q}$ model will be discussed and compared with the decay modes in the QQq model. Finally, Sect. 6 presents the summary and conclusion of this paper.

2 Preliminaries

In this paper, we extend the study of the potential for doubly-heavy tetraquarks from zero temperature [37] to finite temperatures. To begin our discussion on the potential of $QQ\bar{q}\bar{q}$ at finite temperatures, let us first review the specific holographic model utilized in this paper. Following [37, 48, 49], the background metric at finite temperatures is given by:

$$ds^2 = e^{sr^2} \frac{R^2}{r^2} \left(f(r) dt^2 + d\vec{x}^2 + f^{-1}(r) dr^2 \right) + e^{-sr^2} g_{ab}^{(5)} d\omega^a d\omega^b, \tag{1}$$

such model is a deformation of the Euclidean AdS_5 space of radius R , with a deformation parameter s [50]. In the five-dimensional compact space (sphere) characterized by the blackening factor f with coordinates ω^a and $f(r)$, the Nambu–Goto action of a string is expressed as

$$S_{NG} = \frac{1}{2\pi\alpha'} \int_0^1 d\sigma \int_0^T d\tau \sqrt{\gamma}, \tag{2}$$

here, γ represents an induced metric on the string worldsheet with a Euclidean signature, while α' is a parameter associated with the string. For the AdS_5 space, we assume that the blackening factor f takes the form $f(r) = 1 - \left(\frac{r}{r_h}\right)^4$, where $f(0) = 1$ at the boundary and $f(r_h) = 0$ at the horizon. The Hawking temperature, which is consistent with

the temperature of the dual gauge theory, can be defined as $T = \frac{1}{4\pi} |\partial_r f|_{r=r_h}$.

Then, we consider baryon vertices which are string junctions [51]. According to the AdS/CFT correspondence, they are represented by a five-brane wrapped around the internal space X at the point where three strings intersect and appear to be joined together in five dimensions [52, 53]. Correspondingly, the antibaryon vertex is represented by an antibrane in the AdS/CFT correspondence. At leading order α' , the brane’s action is $S_{\text{vert}} = \mathcal{T}_5 \int d^6\xi \sqrt{\gamma^{(6)}}$, where \mathcal{T}_5 represents the brane tension and ξ^i denotes the world-volume coordinates. If we choose static specifications $\xi^0 = t$ and $\xi^a = \theta_a$, where θ_a represents the coordinates on X , then the resulting action is as follows

$$S_{\text{vert}} = \tau_v \int dt \frac{e^{-2sr^2}}{r} \sqrt{f(r)}. \tag{3}$$

Here, \mathcal{T}_v is a dimensionless parameter defined by $\mathcal{T}_v = \mathcal{T}_5 \text{Vol}(X)$, where $\text{vol}(X)$ represents the volume of X , and it serves as a free parameter. Additionally, we have the same action for both baryon and antibaryon vertices $S_{\bar{v}} = S_v$ at finite temperature.

Finally, we consider the light quark located at the end of the string, a scalar field that is coupled to the boundary of the worldsheet via the open string tachyon $S_q = \int d\tau eT$ [54]. Here, the integral is over a world-sheet boundary parameterized by τ , and e is a boundary metric. Assuming a constant background given by $T(x, r) = T_0$ and worldsheets with boundaries along lines in the t direction. Thus, the action can be written as

$$S_q = m \int dt \frac{e^{\frac{s}{2}r^2}}{r} \sqrt{f(r)}. \tag{4}$$

Here, $m = RT_0$ represents the mass of a point particle at rest, with T_0 as its mass. Therefore, the given action describes the behavior of a point particle with mass T_0 at rest. It should be noted that the same action also describes the behavior of light antiquarks located at string endpoints, and hence $S_{\bar{q}} = S_q$. In this model, the interaction of quarks is described by the string tension, which is consistent with Ref. [3].

The model parameters are selected as follows: $g = \frac{R^2}{2\pi\alpha'}$, $k = \frac{r_v}{\frac{3}{g}}$ and $n = \frac{m}{g}$. All our parameters are consistent with Refs. [4, 37, 48, 49] based on the lattice QCD. The value of s is fixed from the slope of the Regge trajectory of $\rho(n)$ mesons in the soft wall model with the geometry Eq. (1). This gives $s = 0.45\text{GeV}^2$. Then, fitting the value of the string tension σ to its value in [39] gives $g = 0.176$. According to the gauge/string duality g is related to the 't Hooft coupling. Next, the parameter m is adjusted to reproduce the lattice result for the $\bar{Q}Q$ string breaking distance $L_c^{(m)}$. With $L_c^{(m)} = 1.22\text{fm}$ [39], it gives $m = 0.538$. The parameter n

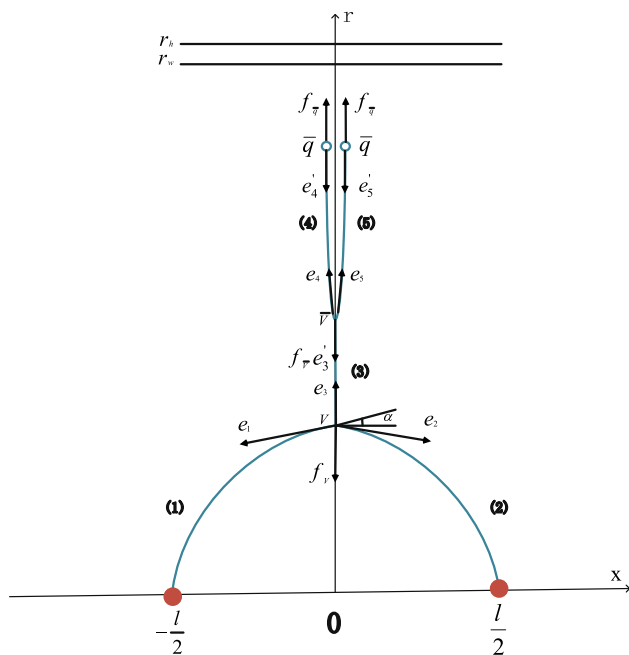


Fig. 1 A static string configuration at small heavy-quark separation distance. The heavy quarks Q are located on the boundary, whereas the light antiquarks \bar{q} , baryon vertex V, and antibaryon vertex \bar{V} are situated in the bulk of the five-dimensional space at $r_{\bar{q}}$, r_v and $r_{\bar{v}}$, respectively. r_h represents the position of the black-hole horizon, while r_w indicates the position of a dynamic wall in the confined phase

is expressed in terms of the parameters of as $n = \frac{m}{g}$ [4]. For fixed the value of k , one should keep in mind two things. First, the value of k can be adjusted to fit the lattice data for the three-quark potential, as is done in [38] for pure $SU(3)$ gauge theory. Unfortunately, at the moment, there are no lattice data available for QCD with two light quarks. Second, the range of allowed values for k is limited to $-\frac{e^3}{15}$ to $-\frac{1}{4}e^{\frac{1}{4}}$. We take $k = -\frac{1}{4}e^{\frac{1}{4}}$ simply because it yields an exact solution to Eq. (20). Finally, the parameters of this article are as follows: $s = 0.45 \text{ GeV}^2$, $g = 0.176$, $n = 3.057$, $k = -\frac{1}{4}E^{\frac{1}{4}}$, and $c = 0.623 \text{ GeV}$ in this model from Ref. [37] at zero temperature. No other extra parameters are introduced in this article.

3 The connected string configuration of $QQ\bar{q}\bar{q}$

3.1 Small L

The configuration of $QQ\bar{q}\bar{q}$ is illustrated in Fig. 1. The total action for this system is given by the sum of the Nambu–Goto actions, as well as the actions associated with the vertices and antiquarks.

$$S = \sum_{i=1}^5 S_{\text{NG}}^{(i)} + 2S_v + 2S_{\bar{q}}. \tag{5}$$

We choose the static gauge $\xi^1 = t$ and $\xi^2 = r$ for the Nambu–Goto actions, the boundary conditions for $x(r)$ become

$$x^{(1)}(0) = -\frac{1}{2}\ell, \quad x^{(2)}(0) = \frac{1}{2}\ell, \quad x^{(1,2,3)}(r_v) = x^{(3,4,5)}(r_{\bar{v}}) = x^{(4,5)}(r_{\bar{q}}) = 0. \tag{6}$$

Considering the boundary conditions, we get the total action

$$S = gT \left(2 \int_0^{r_v} \frac{e^{sr^2}}{r^2} \sqrt{1 + f(r) (\partial_r x)^2} dr + \int_{r_v}^{r_{\bar{v}}} \frac{e^{sr^2}}{r^2} dr + 2 \int_{r_{\bar{v}}}^{r_{\bar{q}}} \frac{e^{sr^2}}{r^2} dr + 3k \frac{e^{-2sr_{\bar{v}}^2}}{r_{\bar{v}}} \sqrt{f(r_{\bar{v}})} + 3k \frac{e^{-2sr_v^2}}{r_v} \sqrt{f(r_v)} + 2n \frac{e^{\frac{1}{2}r_{\bar{q}}^2}}{r_{\bar{q}}} \sqrt{f(r_{\bar{q}})} \right). \tag{7}$$

Here $\partial_r x = \frac{\partial x}{\partial r}$, $T = \int_0^T dt$ and the straight strings are located at $x = 0$. For string (1) and (2), which correspond to the first term in (7), we can derive the equation of motion (EoM) for $x(r)$ using the Euler–Lagrange equation. Thus, it is found that

$$\mathcal{I} = \frac{w(r)f(r)\partial_r x}{\sqrt{1 + f(r) (\partial_r x)^2}}, \quad w(r) = \frac{e^{sr^2}}{r^2}. \tag{8}$$

\mathcal{I} is a constant. We have $\partial_r x = \cot \alpha$ when $r = r_v$, and \mathcal{I} can be expressed as

$$\mathcal{I} = \frac{w(r_v)f(r_v)\partial_r x}{\sqrt{1 + f(r) (\partial_r x)^2}}, \quad w(r) = \frac{e^{sr^2}}{r^2}. \tag{9}$$

Then $\partial_r x$ can be obtained:

$$\begin{aligned} \partial_r x &= \sqrt{\frac{\omega(r_v)^2 f(r_v)^2}{(f(r_v) + \tan^2 \alpha) \omega(r)^2 f(r)^2 - f(r)w(r_v)^2 f(r_v)^2}}. \end{aligned} \tag{10}$$

Using Eq. (10), we can obtain an expression for the separation distance L ,

$$L = 2 \int_0^{r_v} \frac{dx}{dr} dr. \tag{11}$$

Next, we calculate the potential energy of doubly-heavy tetraquark. The energy of string (1) can be got from the first

item in the Eq. (7),

$$E_1 = \frac{S}{T} = \mathbf{g} \int_0^{r_s} \frac{e^{sr^2}}{r^2} dr \sqrt{1 + f(r) (\partial_r x)^2}. \tag{12}$$

This expression is not well-defined, because the integral diverges at $r = 0$. So we should subtract the divergent term

$$E_1 = \frac{S}{T} = \mathbf{g} \int_0^{r_v} \left(\frac{1}{r^2} e^{sr^2} \sqrt{1 + f(r) (\partial_r x)^2} - \frac{1}{r^2} \right) dr - \frac{\mathbf{g}}{r_v} + c, \tag{13}$$

here c is a normalization constant. We can fix the constant by fitting the lattice results. For the heavy quarkonium, we can take $2c$ to fit the potential of heavy quarkonium with lattice. The choice of the normalization constant c for the energy of a single baryon configuration is equal to $3c$. [55] String (2) is calculated in the same way as string (1), and thus $E_1 = E_2$. String (3) is described by the second term in Eq. (7), and represents a straight string stretched between the baryon vertex and antibaryon vertex. The energy can be calculated as

$$E_3 = \frac{S}{T} = \mathbf{g} \int_{r_v}^{r_{\bar{v}}} \frac{e^{sr^2}}{r^2} dr. \tag{14}$$

String (4) and string (5) are both described by the third term in Eq. (7), and represent straight strings.

$$E_4 = E_5 = \frac{S}{T} = \int_{r_{\bar{v}}}^{r_{\bar{q}}} \frac{e^{sr^2}}{r^2} dr. \tag{15}$$

Then, we can get the energy of $QQ\bar{q}\bar{q}$ for this configuration.

$$E_{QQ\bar{q}\bar{q}} = \mathbf{g} \left(2 \int_0^{r_v} \left(\frac{e^{sr^2}}{r^2} \sqrt{1 + f(r) (\partial_r x)^2} - \frac{1}{r^2} \right) dr - \frac{2}{r_v} + \int_{r_v}^{r_{\bar{v}}} \frac{e^{sr^2}}{r^2} dr + 2 \int_{r_{\bar{v}}}^{r_{\bar{q}}} \frac{e^{sr^2}}{r^2} dr + 3k \frac{e^{-2sr_v^2}}{r_v} \sqrt{f(r_v)} + 3k \frac{e^{-2sr_{\bar{v}}^2}}{r_{\bar{v}}} \sqrt{f(r_{\bar{v}})} + 2n \frac{e^{\frac{1}{2}sr_{\bar{q}}^2}}{r_{\bar{q}}} \sqrt{f(r_{\bar{q}})} \right) + 2c. \tag{16}$$

It can be observed from Eq. (16) that energy is a function of r_v , α , and r_h . To obtain the energy of this configuration, we will solve the position of the light antiquark. One crucial condition for equilibrium is that the net forces exerted on the vertices and antiquarks must cancel out. According to the

model, the force (shown in Fig. 1) balance equation in the r direction at $r_{\bar{q}}$ is given by:

$$2f_{\bar{q}} + e'_4 + e'_5 = 0. \tag{17}$$

Here e_i is the string tension [56]. By varying the action with respect to $r_{\bar{q}}$, we get the force $f_{\bar{q}} = \left(0, -\mathbf{g}n \partial_{r_{\bar{q}}} \left(\frac{e^{\frac{1}{2}sr_{\bar{q}}^2}}{r_{\bar{q}}} \sqrt{f(r_{\bar{q}})} \right) \right)$, $e'_4 = e'_5 = \mathbf{g}w(r_{\bar{q}}) (0, -1)$ on the antiquark. Hence, the Eq. (17) becomes

$$-2nsr_{\bar{q}}^2 (f^{\frac{3}{2}}(r_{\bar{q}})) + 2n(f^{\frac{3}{2}}(r_{\bar{q}})) - nr_{\bar{q}} f'(r_{\bar{q}}) - 2f(r_{\bar{q}}) e^{\frac{sr_{\bar{q}}^2}{2}} = 0. \tag{18}$$

$r_{\bar{q}}$ (the position of the light antiquark) is only a function of r_h . This equation gives us the position $r_{\bar{q}}$ at a fixed temperature. Then, at $r_{\bar{v}}$, the force balance equation is

$$f_{\bar{v}} + e'_3 + e_4 + e_5 = 0. \tag{19}$$

Here $f_{\bar{v}}$ is the force on the antibaryon vertex, and each force is determined by

$$f_{\bar{v}} = \left(0, -3 \mathbf{g}k \partial_{r_{\bar{v}}} \left(\frac{e^{-2sr_{\bar{v}}^2}}{r_{\bar{v}}} \sqrt{f(r_{\bar{v}})} \right) \right), \\ e'_3 = \mathbf{g}w(r_{\bar{v}}) (0, -1), \\ e_4 = e_5 = \mathbf{g}w(r_{\bar{v}}) (0, 1).$$

Then, the force balance equation changes

$$\left(4sr_{\bar{v}}^2 + 1 \right) k \sqrt{f(r_{\bar{v}})} e^{-3sr_{\bar{v}}^2} - \frac{1}{2} k r e^{-3sr_{\bar{v}}^2} f'(r_{\bar{v}}) + \frac{1}{3} \sqrt{f(r_{\bar{v}})} = 0. \tag{20}$$

At fixed temperature, $r_{\bar{v}}$ can be determined via the above equation. At r_v , the force balance equation is

$$f_v + e_1 + e_2 + e_3 = 0, \tag{21}$$

here the force on the baryon vertex is $f_v = \left(0, -3 \mathbf{g}k \partial_{r_v} \left(\frac{e^{-2sr_v^2}}{r_v} \sqrt{f(r_v)} \right) \right)$, and the string tensions at the r_v are $e_3 = \mathbf{g}w(r_v) (0, 1)$, $e_1 = \mathbf{g}w(r_v) \left(-\frac{f(r_v)}{\sqrt{\tan^2 \alpha + f(r_v)}}, -\frac{1}{\sqrt{f(r_v) \cot^2 \alpha + 1}} \right)$, $e_2 = \mathbf{g}w(r_v) \left(\frac{f(r_v)}{\sqrt{\tan^2 \alpha + f(r_v)}}, -\frac{1}{\sqrt{f(r_v) \cot^2 \alpha + 1}} \right)$. α is the angle shown in Fig. 1. Putting these forces into Eq. (21), the force balance equation becomes

$$\left(4sr_v^2 + 1 \right) k \sqrt{f(r_v)} e^{-3sr_v^2} - \frac{1}{2} k r e^{-3sr_v^2} f'(r_v)$$

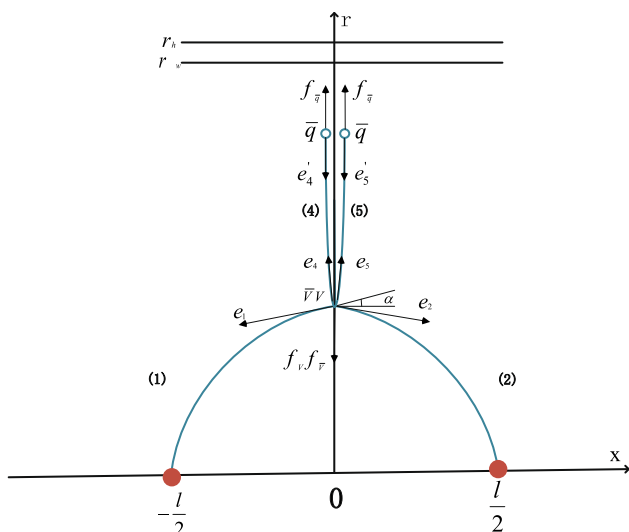


Fig. 2 A static configuration is formed by a slightly larger separation distance of a heavy-quark pair. The baryon vertex and the antibaryon vertex are in the same position. The force acting on the point is indicated by the black arrow

$$+ \frac{1}{3} \sqrt{f(r_v)} \left(1 - \frac{2}{\sqrt{f(r_v) \cot^2 \alpha + 1}} \right) = 0. \tag{22}$$

By taking the variation of the action with respect to r_v , we can deduce the relationship between r_v and α .

3.2 Slightly larger L

The second configuration is shown in Fig. 2, and we consider the second configuration as one in which a string (3) contracts to a single point. The total action is now expressed by

$$S = \sum_{i=1, i \neq 3}^5 S_{\text{NG}}^{(i)} + 2S_v + 2S_{\bar{q}}. \tag{23}$$

We choose the same static gauge as before and the boundary conditions are

$$\begin{aligned} x^{(1)}(0) &= -\frac{1}{2} \ell, & x^{(2)}(0) &= \frac{1}{2} \ell, \\ x^{(i)}(r_v) &= x^{(4,5)}(r_{\bar{q}}) = 0. \end{aligned} \tag{24}$$

The separation distance of the slightly larger L is still determined by Eq. (11), which is the same as that used for the small L . Compared to the first configuration, the string (3) in the second configuration contracts to a point. Therefore, we need to consider other string tensions that satisfy Eqs. (13)–(15). Then, the energy of the slightly larger L can be expressed as

$$\begin{aligned} E_{QQ\bar{q}\bar{q}} &= g \left(2 \int_0^{r_v} \left(\frac{e^{sr^2}}{r^2} \sqrt{1 + f(r)} (\partial_r x)^2 - \frac{1}{r^2} \right) dr \right. \\ &\quad - \frac{2}{r_v} + 2 \int_{r_v}^{r_{\bar{q}}} \frac{e^{sr^2}}{r^2} dr + 3k \frac{e^{-2sr_v^2}}{r_v} \sqrt{f(r_v)} \\ &\quad \left. + 3k \frac{e^{-2sr_{\bar{v}}^2}}{r_{\bar{v}}} \sqrt{f(r_{\bar{v}})} + 2n \frac{e^{\frac{1}{2}sr_{\bar{q}}^2}}{r_{\bar{q}}} \sqrt{f(r_{\bar{q}})} \right) + 2c. \end{aligned} \tag{25}$$

As before, we will now proceed with solving the force balance equation. The location of $r_{\bar{q}}$ can be determined using Eq. (18). Then, the force balance equation at the point $r = r_v = r_{\bar{v}}$ is

$$f_v + f_{\bar{v}} + e_1 + e_2 + e_4 + e_5 = 0. \tag{26}$$

Each force is determined by

$$\begin{aligned} f_v = f_{\bar{v}} &= \left(0, -3gk \partial_{r_v} \left(\frac{e^{-2sr_v^2}}{r_v} \sqrt{f(r_v)} \right) \right), \\ e_1 &= gw_{(r_v)} \left(-\frac{f(r_v)}{\sqrt{\tan^2 \alpha + f(r_v)}}, -\frac{1}{\sqrt{f(r_v) \cot^2 \alpha + 1}} \right), \\ e_2 &= gw_{(r_v)} \left(\frac{f(r_v)}{\sqrt{\tan^2 \alpha + f(r_v)}}, -\frac{1}{\sqrt{f(r_v) \cot^2 \alpha + 1}} \right), \\ e_4 = e_5 &= gw_{(r_v)} (0, 1). \end{aligned}$$

Then, the Eq. (26) becomes

$$\begin{aligned} (24sr_v^2 f(r_v) + 6f(r_v) - 3rf'(r_v)) ke^{-3sr_v^2} \\ - \frac{2}{\sqrt{f(r_v) \cot^2 \alpha + 1}} + 2\sqrt{f(r_v)} = 0. \end{aligned} \tag{27}$$

3.3 Intermediate L

The third configuration, as shown in Fig. 3, is characterized by the compression of points $r_{\bar{q}}$, $r_{\bar{v}}$ and r_v into a single location. The configuration of the total action is given by

$$S = \sum_{i=1}^2 S_{\text{NG}}^{(i)} + 2S_v + 2S_{\bar{q}}. \tag{28}$$

Choosing the static gauge in the Nambu–Goto actions as before, then the boundary conditions can be obtained

$$x^{(1)}(0) = -\frac{1}{2} \ell, \quad x^{(2)}(0) = \frac{1}{2} \ell, \quad x^{(i)}(r_v) = 0. \tag{29}$$

Equation (11) gives us the separation distance in this configuration. To calculate the energies, we only need to consider

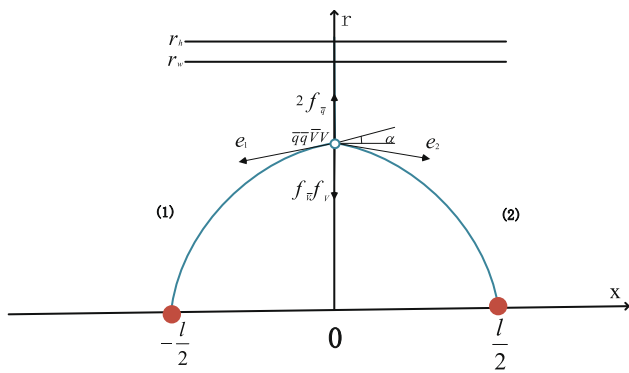


Fig. 3 Static configuration at an intermediate separation distance of a heavy-quark pair. The baryon vertex, antiquark and the antibaryon vertex are in the same position. The force acting on the point is indicated by the black arrow

the range from $r = 0$ to $r = r_v$, as specified by Eq. (13). Naturally, the energy of the configuration is

$$E_{QQ\bar{q}\bar{q}} = g \left(2 \int_0^{r_v} \left(\frac{e^{sr^2}}{r^2} \sqrt{1 + f(r)} (\partial_r x)^2 - \frac{1}{r^2} \right) dr - \frac{2}{r_v} + 6k \frac{e^{-2sr_v^2}}{r_v} \sqrt{f(r_v)} + 2n \frac{e^{\frac{1}{2}sr_{\bar{q}}^2}}{r_{\bar{q}}} \sqrt{f(r_{\bar{q}})} \right) + 2c. \tag{30}$$

The force balance equation at the point $r = r_v = r_{\bar{v}} = r_{\bar{q}}$ is

$$f_v + f_{\bar{v}} + 2f_{\bar{q}} + e_1 + e_2 = 0. \tag{31}$$

Each force is determined by

$$f_v = f_{\bar{v}} = \left(0, -3gk \partial_{r_v} \left(\frac{e^{-2sr_v^2}}{r_v} \sqrt{f(r_v)} \right) \right),$$

$$e_1 = gw_{(r_v)} \left(-\frac{f(r_v)}{\sqrt{\tan^2 \alpha + f(r_v)}}, -\frac{1}{\sqrt{f(r_v) \cot^2 \alpha + 1}} \right),$$

$$e_2 = gw_{(r_v)} \left(\frac{f(r_v)}{\sqrt{\tan^2 \alpha + f(r_v)}}, -\frac{1}{\sqrt{f(r_v) \cot^2 \alpha + 1}} \right),$$

$$f_{\bar{q}} = \left(0, -gn \partial_{r_{\bar{q}}} \left(\frac{e^{\frac{1}{2}sr_{\bar{q}}^2}}{r_{\bar{q}}} \sqrt{f(r_{\bar{q}})} \right) \right).$$

Here $r_{\bar{q}} = r_{\bar{v}} = r_v$, then, the Eq. (31) becomes

$$ke^{-2sr_v} (24sr_v^2 f(r_v) + 6f(r_v) - 3r_v f'(r_v)) + ne^{\frac{1}{2}sr_v^2} (2f(r_v) - 2sr_v^2 f(r_v) - r_v f'(r_v)) - \frac{2\sqrt{f(r)} e^{sr_v^2}}{\sqrt{f(r_v) \cot^2 \alpha + 1}} = 0. \tag{32}$$

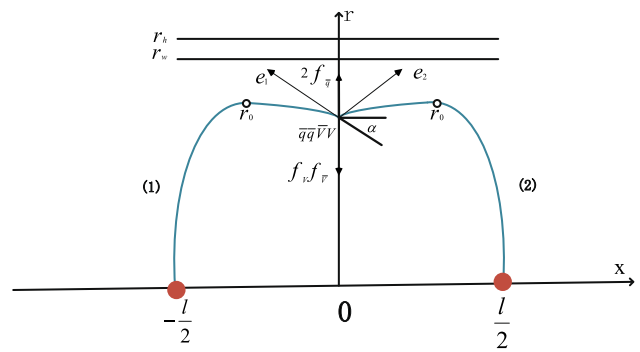


Fig. 4 Static configuration at a large separation distance of a heavy-quark pair. There are two turning points at strings (1) and (2) and they are symmetric about the Y-axis. The force acting on the point is indicated by the black arrow

3.4 Large L

Figure 4 illustrates the fourth configuration. The total action for this configuration, denoted as intermediate L, is given by Eq. (28). We choose another static gauge $\xi^1 = t$ and $\xi^2 = x$ in the Nambu–Goto actions and the boundary conditions are

$$r^{(1)}(-L/2) = r^{(2)}(L/2) = 0, \quad r^{(i)}(0) = r_v. \tag{33}$$

Then, the total action becomes

$$S = gT \left(\int_{-L/2}^0 \frac{e^{sr^2}}{r^2} \sqrt{f(r) + (\partial_r x)^2} dx + \int_0^{L/2} \frac{e^{sr^2}}{r^2} \sqrt{f(r) + (\partial_r x)^2} dx + 6k \frac{e^{-2sr_v^2}}{r_v} \sqrt{f(r_v)} + 2n \frac{e^{-\frac{1}{2}sr_{\bar{q}}^2}}{r_{\bar{q}}} \sqrt{f(r_{\bar{q}})} \right). \tag{34}$$

The action for string (1) is given by the first term in Eq. (34). The subsequent step is to compute the first integral.

$$\mathcal{I} = \frac{w(r) f(r)}{\sqrt{f(r) + (\partial_x r)^2}}. \tag{35}$$

\mathcal{I} is a constant. At the r_0 and r_v points, we can obtain, respectively

$$\frac{w(r) f(r)}{\sqrt{f(r) + (\partial_x r)^2}} = w(r_0) \sqrt{f(r_0)}. \tag{36}$$

$$\frac{w(r_v) f(r_v)}{\sqrt{f(r_v) + \tan^2 \alpha}} = w(r_0) \sqrt{f(r_0)}. \tag{37}$$

Here $\partial_x r$ can be obtained from Eqs. (36), (37)

$$\partial_x r = \sqrt{\frac{w(r)^2 f(r)^2 f(r_0) - f(r)w(r_0)^2 f(r_0)^2}{w(r_0)^2 f(r_0)^2}}. \tag{38}$$

The large L configuration has a turning point at r_0 , so the distance between heavy quarks is calculated in two parts. Then, the separation distance can be expressed as

$$L = 2(L_1 + L_2) = 2\left(\int_0^{r_0} \frac{1}{r'} dr + \int_{r_v}^{r_0} \frac{1}{r'} dr\right). \tag{39}$$

Here r' denotes $\partial_x r$. By substituting Eq. (38) into Eq. (39), the separation distance can be obtained. The energy of string (1) was calculated in two parts, which is similar to the separation distance. Therefore, the energy of string (1) is given by

$$E_1 = E_{R_1} + E_{R_2} = \mathbf{g} \int_0^{r_0} w(r) \sqrt{1 + f(r)x'^2} dr + \mathbf{g} \int_{r_{\bar{q}}}^{r_0} w(r) \sqrt{1 + f(r)x'^2} dr. \tag{40}$$

Same as the case of small L , we also need to subtract the divergent term here. Thus, Eq. (40) can be expressed as

$$E_1 = \mathbf{g} \int_0^{r_0} \left(w(r) \sqrt{1 + f(r)x'^2} - \frac{1}{r^2} \right) dr + \mathbf{g} \int_{r_v}^{r_0} w(r) \sqrt{1 + f(r)x'^2} dr - \frac{1}{r_0} + 2c. \tag{41}$$

String (2) is calculated in the same way as string (1). Therefore, the total energy of the configuration is

$$E_{QQ\bar{q}\bar{q}} = 2\mathbf{g} \int_0^{r_0} \left(w(r) \sqrt{1 + f(r)x'^2} - \frac{1}{r^2} \right) dr + 2\mathbf{g} \int_{r_v}^{r_0} w(r) \sqrt{1 + f(r)x'^2} dr - \frac{2\mathbf{g}}{r_0} + 6kg \frac{e^{-2sr_{\bar{v}}}}{r_{\bar{v}}} \sqrt{f(r_{\bar{v}})} + 2ng \frac{e^{\frac{1}{2}sr_{\bar{q}}^2}}{r_{\bar{q}}} \sqrt{f(r_{\bar{q}})} + 2c. \tag{42}$$

The force balance equation is the same as that for intermediate L , and the expressions of force are also the same as intermediate L . Equation (37) represents the functional relationship between r_v and α when the temperature is fixed. We can first solve Eqs. (32) and (37), and then substitute the numerical values into Eqs. (39) and (42) to obtain the solutions for L and $E_{QQ\bar{q}\bar{q}}$. For α , at small separate distance of heavy quarks, as r_v increases, the distance between the heavy quarks increases, and the curvature of the string between heavy quarks increases, causing α to decrease. When the string reaches $\alpha = 0$ and r_v increases further, the string will become an M-shape, at which point α becomes negative.

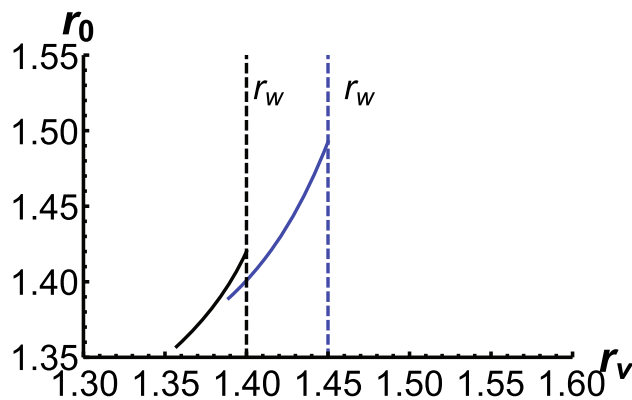


Fig. 5 r_0 as a function of r_v in the larger L configuration, where the black line is r_0 at $T = 0$, while the blue line is r_0 at $T = 0.08$ GeV. r_w indicates the position of a dynamic wall

4 Numerical results and discussion

4.1 T = 0.08 GeV

At a low temperature of 0.08 GeV, the configurations of $QQ\bar{q}\bar{q}$ are confined. Below the black-hole horizon, there exists a dynamic wall that prevents the string from crossing. In this part, we investigate four configurations of $QQ\bar{q}\bar{q}$ at this temperature.

First, we will give a discussion about the dynamic wall at finite temperature. Different from the quark–antiquark pair, the configuration of $QQ\bar{q}\bar{q}$ shows a “M” shape at large separation distance. Thus, the maximum value of r_0 at infinite separation distance gives the position of dynamic wall. By calculating the position of the dynamic wall, we obtain $r_w = 1.40 \text{ GeV}^{-1}$ at $T = 0$ and $r_w = 1.45 \text{ GeV}^{-1}$ at $T = 0.08$ GeV as shown in Fig.5. The increase of temperature leads to an increase of the position of dynamic wall in the r direction.

For small L , we use Eq. (18) to calculate the position of the antiquark. The result shows that at a temperature of 0.08 GeV, $r_{\bar{q}} = 1.13 \text{ GeV}^{-1}$. Subsequently, the antibaryon vertex position can be calculated using Eq. (20), which yields $r_{\bar{v}} = 0.445 \text{ GeV}^{-1}$. Within the range of $0 < r < r_v$, we can calculate α using Eq. (22), as illustrated in Fig.6. It can be observed that α exhibits a decreasing trend as r_v increases. Then, the separation distance of a heavy-quark pair and its corresponding energy can then be obtained using Eqs. (11) and (16), respectively. These results are presented in Fig. 10 and Fig. 11.

When r_v increases to $r_{\bar{v}}$, it reaches a critical value and transitions to the second configuration. In the second configuration, we can still determine the position of antiquark using Eq. (18). Subsequently, we use Eq. (27) to obtain α , as depicted in Fig.7. α exhibits an increasing trend as r_v increases, reaching its peak when $r_v = r_{\bar{v}}$. Next, we can

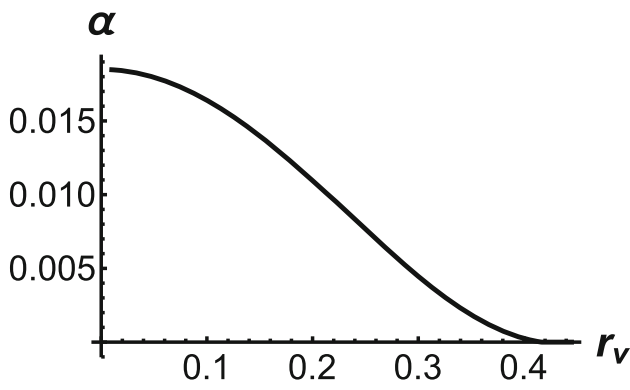


Fig. 6 α as a function of r_v in the small L configuration. The unit for r_v is GeV^{-1}

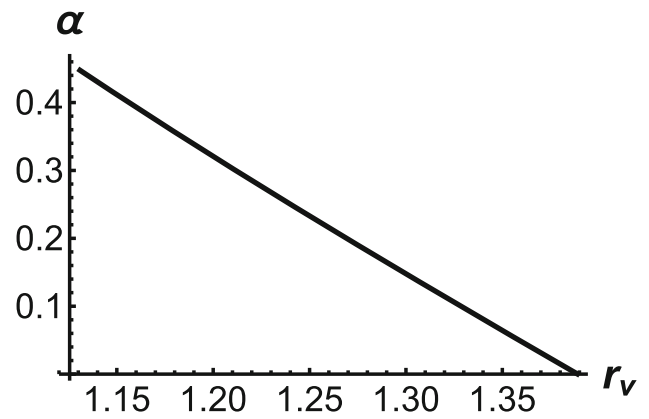


Fig. 8 α as a function of r_v in the intermediate L configuration. The unit for r_v is GeV^{-1}

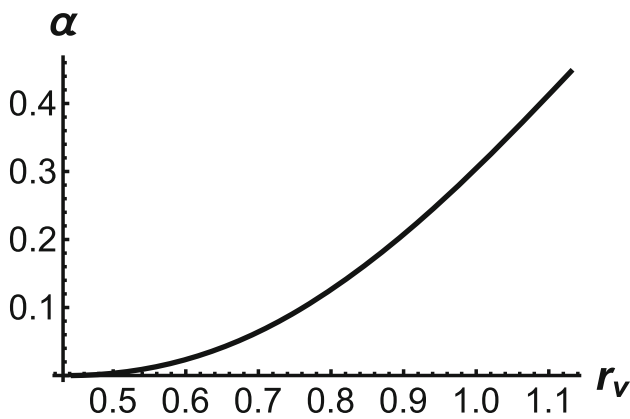


Fig. 7 α as a function of r_v in the slightly larger L configuration. The unit for r_v is GeV^{-1}

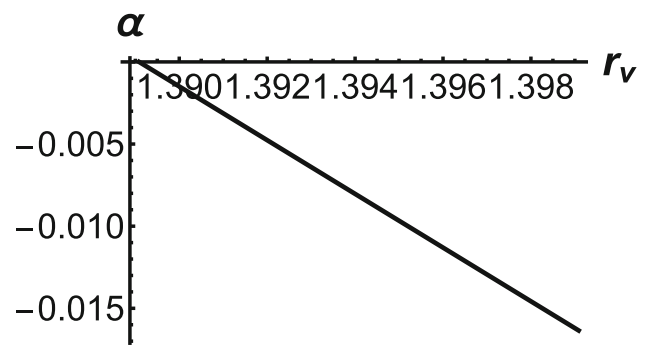


Fig. 9 α as a function of r_v in the large L configuration. The unit for r_v is GeV^{-1}

obtain the separation distance and energy of the second configuration using Eqs. (11) and (25), and it is observed that as r_v increases, L and E also exhibit an upward trend. When r_v reaches $r_{\bar{v}}$, it attains its maximum value. Beyond this point, the configuration switches to the third configuration.

In the third configuration, $r_{\bar{v}}$ overlaps with the $r_{\bar{q}}$ point. Using Eq. (32), we can establish a functional relationship between r_v and α , as shown in Fig. 8. Clearly, α exhibits a linear decrease with increasing r_v until it reaches 0. E and L can be obtained using Eqs. (11) and (30). In this configuration, E varies linearly with L . When r_v exceeds $r_{\bar{q}}$, the configuration shifts into the fourth configuration.

Then, in the configuration with large L , as r_v increases below the dynamic wall, strings (1) and (2) exhibit turning points. α continues to decrease as r_v increases, as shown in Fig. 9. However, unlike before, α becomes negative. As shown in Fig. 9, the maximum value of r_v is 1.40 GeV^{-1} , which corresponds to the position of the dynamic wall at $r_w \approx r_0 \approx 1.45 \text{ GeV}^{-1}$. We can obtain E and L using Eqs. (39) and (42).

At $T = 0.08 \text{ GeV}$, the separation distance and energy plots for the tetraquark configuration are illustrated in

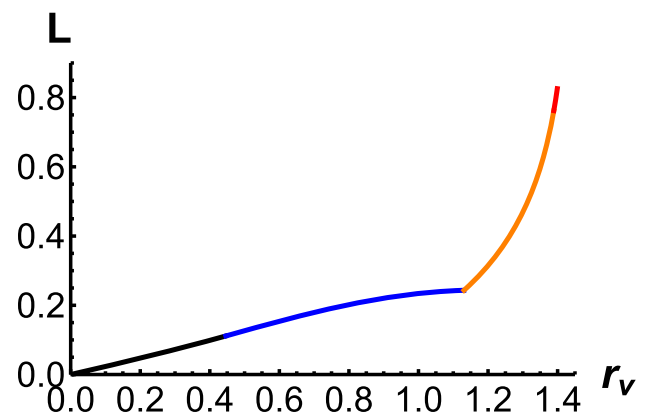


Fig. 10 Separation distance L as a function of r_v , where the black line represents the configuration with small L , blue represents slightly larger L , orange represents intermediate L , and red represents larger L . The unit of L is in fm and that of r_v is in GeV^{-1}

Figs. 10 and 11, respectively. As can be observed from the figure, there is a smooth connection of L for each configuration. As r_v increases, L also approaches infinity. This implies that r_v cannot be infinite, and when the maximum value is exceeded, the configuration will decay into another state. We will discuss this further in the upcoming section. The energy

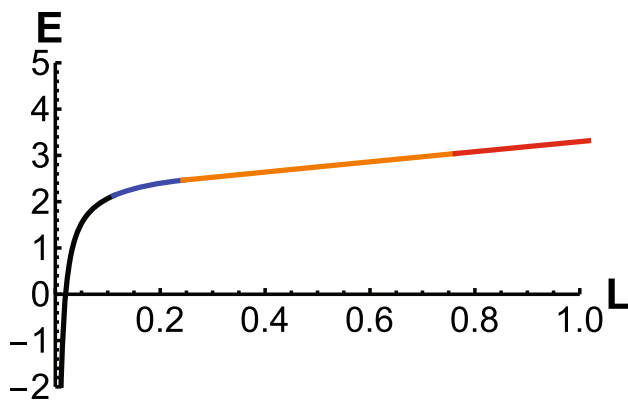


Fig. 11 Energy E as a function of separation distance L at $T = 0.08$ GeV. The black line represents the configuration with small L , blue line represents slightly larger L , orange line represents intermediate L , and red line represents larger L . The unit of E is in GeV and that of r_v is in GeV^{-1}

increases as the separation distance increases. Notably, the energy is dominated by Coulomb potential at small separation distances and linear potential at large distances.

4.2 $T = 0.115$ GeV

At a temperature of $T = 0.115$ GeV, the configurations of $QQ\bar{q}\bar{q}$ are deconfined. For a deconfined $QQ\bar{q}\bar{q}$, the melting of $QQ\bar{q}\bar{q}$ can happen at a certain separation distance. If the separation distance of heavy quark–antiquark pair is small enough, the $QQ\bar{q}\bar{q}$ will not melt even at high temperature. When increasing the distance of heavy quark–antiquark pair, the color screening becomes important and the $QQ\bar{q}\bar{q}$ will melt. In summary, the dynamic wall disappears and $QQ\bar{q}\bar{q}$ will melt at a sufficiently far distance in this stage.

Firstly, similar to $T = 0.08$ GeV, we focus on the first configuration. The position of the antiquark can be determined using Eq. (18), which yields $r_{\bar{q}} = 1.1677 \text{ GeV}^{-1}$ when $T = 0.115$ GeV. Next, we can calculate the position of the antibaryon vertex using Eq. (20), which yields $r_{\bar{v}} = 0.4626 \text{ GeV}^{-1}$, and then use Eq. (22) to determine α . L and E can still be obtained from Eqs. (11) and (16), respectively. We can then proceed to investigate the second and third configurations using a similar approach as the $T = 0.08$ GeV calculation. This will enable us to determine the separation distance and energy. As the value of r_v continues to increase, the value of L also exhibits a tendency to increase. However, as L approaches a maximum value, it will tend towards infinity, indicating that the quark is now free and large L configurations will no longer be possible as shown in Fig. 12 [57–59]. First, similar to $T = 0.08$ GeV, we focus on the first configuration. The position of the antiquark can be determined using Eq. (18), which yields $r_{\bar{q}} = 1.1677 \text{ GeV}^{-1}$ when $T = 0.115$ GeV. Next, we can calculate the position of the antibaryon vertex using Eq. (20), which yields $r_{\bar{v}} = 0.4626 \text{ GeV}^{-1}$,

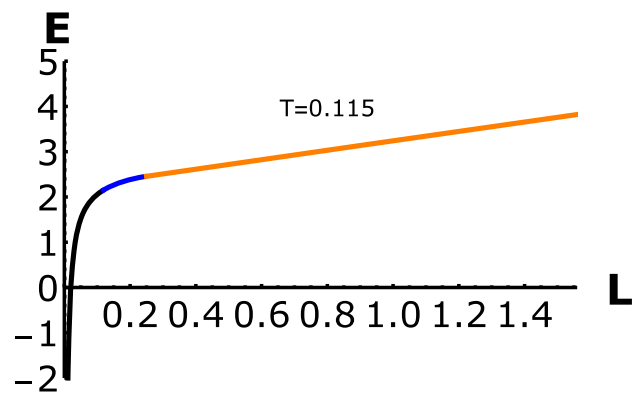


Fig. 12 Energy E as a function of separation distance L at $T = 0.115$ GeV. The black line represents the configuration with small L , blue line represents slightly larger L and orange line represents intermediate L . The unit of E is in GeV and that of r_v is in GeV^{-1}

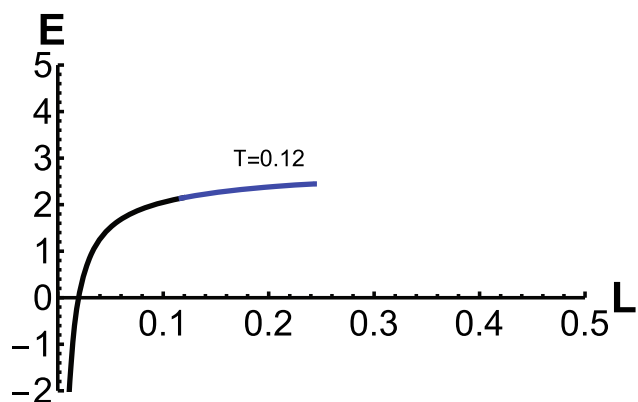


Fig. 13 Energy E as a function of separation distance L at $T = 0.12$ GeV. The black line represents the configuration with small L and blue line represents slightly larger L . The unit of E is in GeV and that of r_v is in GeV^{-1}

and then use Eq. (22) to determine α . L and E can still be obtained from Eqs. (11) and (16), respectively. Subsequently, we can investigate the second and third configurations at this temperature by adopting the same method as the $T = 0.08$ GeV calculation, which allows us to determine the separation distance of heavy quarks and energy. As the value of r_v continues to increase, the value of L also exhibits a tendency to increase. However, as L approaches a maximum value ($L_{max} = 1.56\text{fm}$), it will tend towards infinity, indicating that the quark is now free and large L configurations will no longer be possible [57–59]. The diagram of energy and separation distance is shown in Fig. 12.

4.3 $T = 0.12$ GeV

To begin with, we can use Eq. (18) to determine the position of the antiquark, which is $r_{\bar{q}} = 1.1785 \text{ GeV}^{-1}$ when $T = 0.12$ GeV. Next, we can use Eq. (20) to calculate the position of the antibaryon vertex, which yields $r_{\bar{v}} = 0.46574$

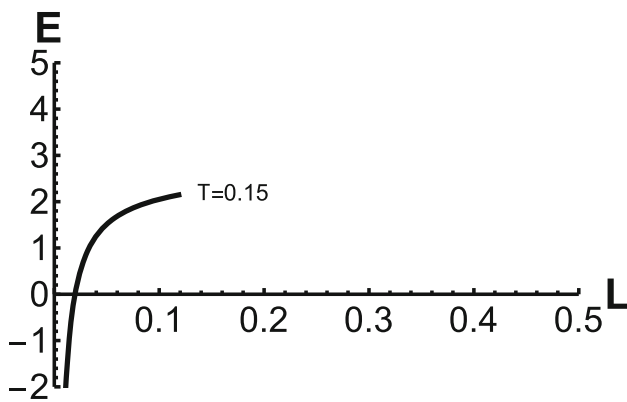


Fig. 14 Energy E as a function of separation distance L at $T = 0.15$ GeV. The black line represents the configuration with small L . The unit of E is in GeV and that of r_v is in GeV^{-1}

GeV^{-1} . Following this, we can similarly obtain functional expressions for α , L , and E as r_v increased, which are illustrated in Fig. 13. As depicted in the figure, both L and E exhibit linear growth with respect to r_v , and the energy function E shows a Cornell-like potential. At slightly larger L , Eqs. (11) and (25) are employed to calculate the separation distance and energy. However, at this temperature, as r_v keeps increasing, the configuration will eventually collapse, leading to the quark becoming a free state. Therefore, there exists a maximum value of L , beyond which L will tend towards infinity. Consequently, large values of L are not possible at this temperature.

4.4 $T = 0.15$ GeV

At this temperature, using the force balance equation, the position of the quark or antibaryon vertex is determined to be $r_{\bar{v}} = 0.4726 \text{ GeV}^{-1}$. However, we have discovered that at this temperature there is no solution for the position of the antiquark, $r_{\bar{q}}$. Therefore, we have computed the separation distance and energy for the first configuration, which are displayed in Fig. 14. As $r_{\bar{v}}$ surpasses a certain value, the $QQ\bar{q}\bar{q}$ configuration collapses, resulting in the quark becoming free.

4.5 Short summary

Based on the calculation results of the $QQ\bar{q}\bar{q}$ potential at the above mentioned four temperatures, it shows that both $r_{\bar{q}}$ and $r_{\bar{v}}$ become larger and gradually approach the position of the dynamic wall as the temperature increases. Furthermore, the melting of the $QQ\bar{q}\bar{q}$ configuration happens at a small distance as the temperature increases. Comparing the two lines for $T = 0$ and $T = 0.11$ GeV in Fig. 15, we observe that as temperature increases, the same separation distance L corresponds to a lower energy value. Besides, at small distances, $QQ\bar{q}\bar{q}$ exhibits Coulombic behavior, whereas at

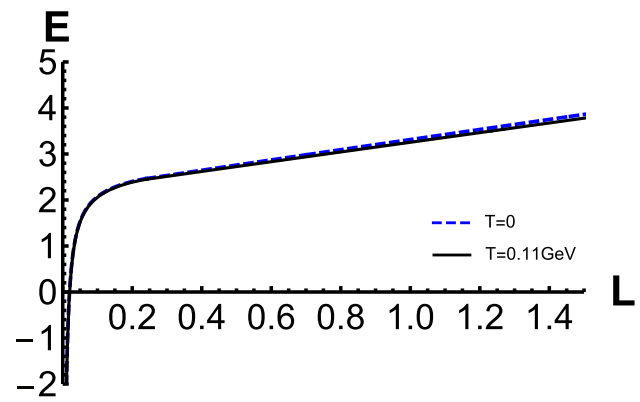


Fig. 15 The blue dash line is the energy at zero temperature, while the black line is the energy at $T = 0.11$ GeV

large distances, the behavior is linear at finite temperature [60–62].

5 Decay modes

5.1 $QQ\bar{q}\bar{q}$

During the confinement phase, quarks are confined within hadrons. However, as the distance between heavy quarks increases, the strings connecting them eventually break [63]. In this context, we shall consider three decay modes for $QQ\bar{q}\bar{q}$ configurations.

$$\begin{aligned}
 & \nearrow Q\bar{q} + Q\bar{q} \\
 QQ\bar{q}\bar{q} & \rightarrow QQq + \bar{q}\bar{q}\bar{q} \\
 & \searrow Qq\bar{q}\bar{q} + Q\bar{q}.
 \end{aligned}
 \tag{43}$$

Figure 16 displays the configuration diagram for the three possible decay modes. We will proceed to analyze the energy of each disconnected configuration. $Q\bar{q}$ consists of a fundamental string and an antiquark, with the total action given by $S_{Q\bar{q}} = S_{\text{NG}} + S_q$. QQq comprises two strings, a vertex, and a light quark. The total action can be written as $S_{QQq} = \sum_{i=1}^2 S_{\text{NG}}^{(i)} + S_{\text{vert}} + S_{\bar{q}}$. On the other hand, $Q\bar{q}\bar{q}\bar{q}$ consists of four strings, a vertex, an antibaryon vertex, a light quark and two antiquarks. The total action is $S_{Q\bar{q}\bar{q}\bar{q}} = \sum_{i=1}^4 S_{\text{NG}}^{(i)} + S_v + S_{\bar{v}} + 2S_{\bar{q}} + S_q$. Furthermore, $\bar{q}\bar{q}\bar{q}$ consists of an antibaryon vertex and three antiquarks, with the total action $S_{\bar{q}\bar{q}\bar{q}} = S_{\bar{v}} + 3S_{\bar{q}}$. We employ the same static gauge as before and obtain the total action for each configuration by specifying appropriate boundary conditions. The detailed calculation process of the energy of each configuration is given in Refs. [48,49,55,56]. Subsequently, The

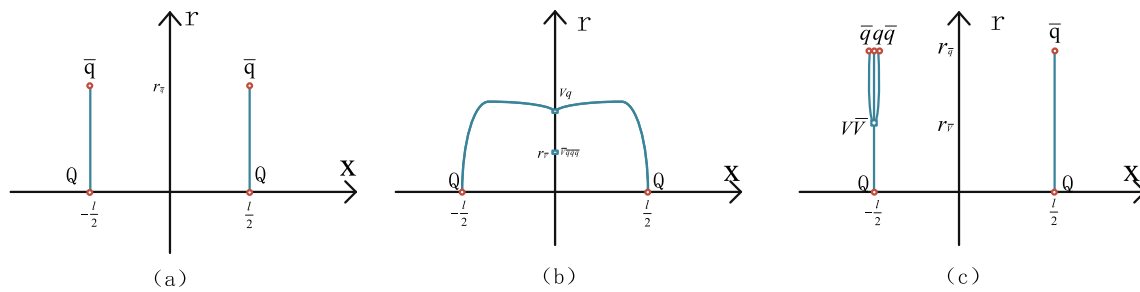


Fig. 16 Three disconnected configuration of $QQ\bar{q}\bar{q}$

action of each decay is then calculated.

$$\begin{aligned}
 S_1 &= S_{Q\bar{q}} + S_{Q\bar{q}} \\
 S_2 &= S_{QQq} + S_{\bar{q}\bar{q}\bar{q}} \\
 S_3 &= S_{QQ\bar{q}\bar{q}} + S_{Q\bar{q}}
 \end{aligned}
 \tag{44}$$

The results of the calculation are shown in Fig. 17. Here, we define the string-breaking distance as the intersection point of the two energies. As shown in Fig. 17b, we can see that when $L_{QQ\bar{q}\bar{q}} = 0.1870$ fm, $QQ\bar{q}\bar{q}$ will decay into $Q\bar{q} + Q\bar{q}$, and when $L_{QQ\bar{q}\bar{q}} = 1.3036$ fm, $QQ\bar{q}\bar{q}$ will decay into $QQq + Q\bar{q}$. However, at zero temperature (as shown in Fig. 17a), the former decay takes place at $L_{QQ\bar{q}\bar{q}} = 0.1874$ fm, while the latter occurs at $L_{QQ\bar{q}\bar{q}} = 1.3147$ fm. The first scenario is linked to the process of vertex annihilation, whereas the second pertains to the occurrence of string breaking through the production of light quark pairs. The $QQ\bar{q}\bar{q} \rightarrow Q\bar{q} + Q\bar{q}$ is the most possible decay mode. The presence of small temperature will increase the string-breaking distance a little bit. There is always a energy difference for $QQ\bar{q}\bar{q}$ and $QQq + \bar{q}\bar{q}\bar{q}$ as shown in Fig. 17. Thus, the decay mode $QQ\bar{q}\bar{q} \rightarrow QQq + \bar{q}\bar{q}\bar{q}$ also will not happen.

5.2 The relation between QQq and $QQ\bar{q}\bar{q}$

In this part, we will discuss the difference between $QQ\bar{q}\bar{q}$ and QQq at a temperature of 0.08 GeV. The QQq configuration has also garnered widespread attention. Similar to the $QQ\bar{q}\bar{q}$ configuration, the decay process $QQq \rightarrow Qqq + Q\bar{q}$ will occur in the QQq configuration at high temperatures. As shown in Fig. 18, we calculated the two configurations separately as well as the energy after their decay. Then, $QQ\bar{q}\bar{q}$ decays to $Q\bar{q}$ at $E = 2.3806$ GeV ($L = 0.1980$ fm), and QQq decays to $Qqq + Q\bar{q}$ at $E = 3.0167$ GeV ($L = 1.2646$ fm). At lower energies and smaller separation distances, the $QQ\bar{q}\bar{q}$ configuration will decay, while QQq is more stable. This difference may result from two distinct mechanisms: string breaking by light quarks for QQq and string junction annihilation for $QQ\bar{q}\bar{q}$.

Here, we also consider another relation in [29,37], which is $E_{QQ\bar{q}\bar{q}} = E_{QQq} + E_{Qqq} - E_{q\bar{q}}$. This relationship is derived from heavy quark–diquark symmetry, as illustrated in Fig. 19. Furthermore, similar to the case at zero temperature, we find that relationship occurs at a very small separation distance when $T = 0.08$ GeV. After $L = 0.2662$ fm, the potential energy of $QQ\bar{q}\bar{q}$ and $QQq + Qqq - q\bar{q}$ continues to increase. So there’s a slight difference in energy, specifically, the energy of $QQq + Qqq - q\bar{q}$ will be slightly higher than that of $QQ\bar{q}\bar{q}$. In addition, we find that the energy difference between before and after equation will occur after $L = 0.2396$ fm when it is at zero temperature, and after $L = 0.2662$ fm when it is at $T = 0.08$ GeV. The increase in temperature will increase the critical distance for the appearance of energy difference.

6 Summary and conclusion

This paper focuses on the melting and breaking of strings in $QQ\bar{q}\bar{q}$ at finite temperatures by using the five-dimensional effective string model, and compares it with QQq under same conditions. During the confinement phase, a dynamic wall which strings cannot penetrate forms below the black-hole horizon. As the temperature increases, the system enters the deconfinement phase. In this phase, the dynamic wall disappears, causing the $QQ\bar{q}\bar{q}$ string to melt and the quarks to become free. We investigate the energy of $QQ\bar{q}\bar{q}$ at which string melting occurs at four different temperatures. Subsequently, the study of three decay modes of $QQ\bar{q}\bar{q}$ configuration at high temperature is continued, and the temperature at which the different decay modes occur is calculated. Finally, we compare the decay model of the $QQ\bar{q}\bar{q}$ configuration at $T = 0.08$ GeV with that of the QQq and conclude that the QQq configuration is more stable under the same conditions. Ultimately, we aim to provide additional insights for experiments through our study of the effective string model in the future work.

Acknowledgements This work is supported by the Natural Science Foundation of Hunan Province of China under Grants No. 2022JJ40344, the Research Foundation of Education Bureau of Hunan Province,

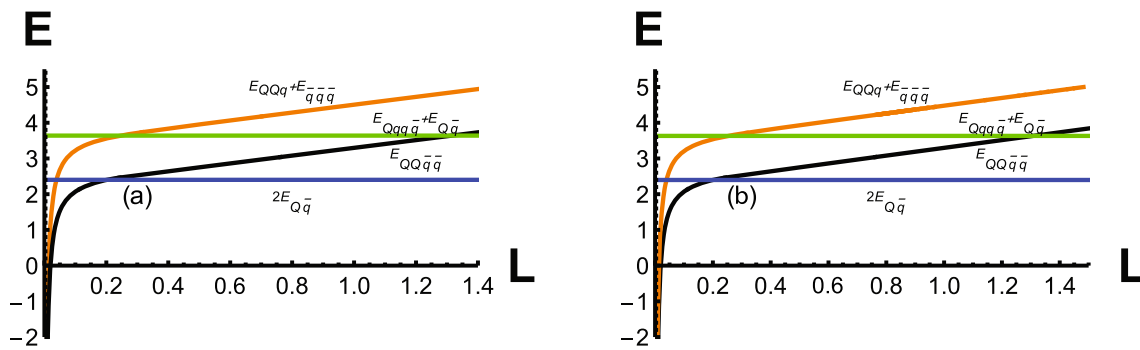


Fig. 17 a $QQ\bar{q}\bar{q}$ and his three disconnected configuration energy at temperature $T = 0$ GeV. b $QQ\bar{q}\bar{q}$ and his three disconnected configuration energy at temperature $T = 0.08$ GeV. The black line is the

energy of $E_{QQ\bar{q}\bar{q}}$, the blue line is the energy of $2E_{Q\bar{q}}$, the orange line is the energy of $E_{QQq} + E_{\bar{q}\bar{q}}$, and the green line is the energy of $E_{QQq\bar{q}} + E_{Q\bar{q}}$

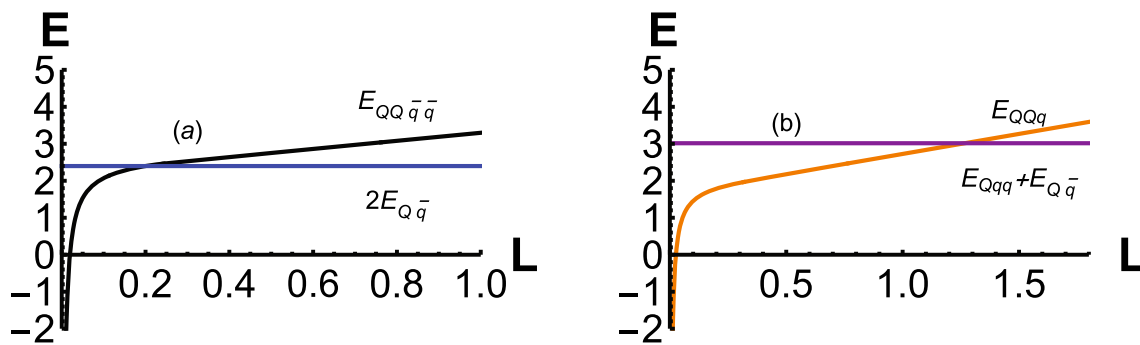


Fig. 18 a The energy of the $QQ\bar{q}\bar{q}$ and two $Q\bar{q}$. b The energy of the QQq and $Qq + Q\bar{q}$

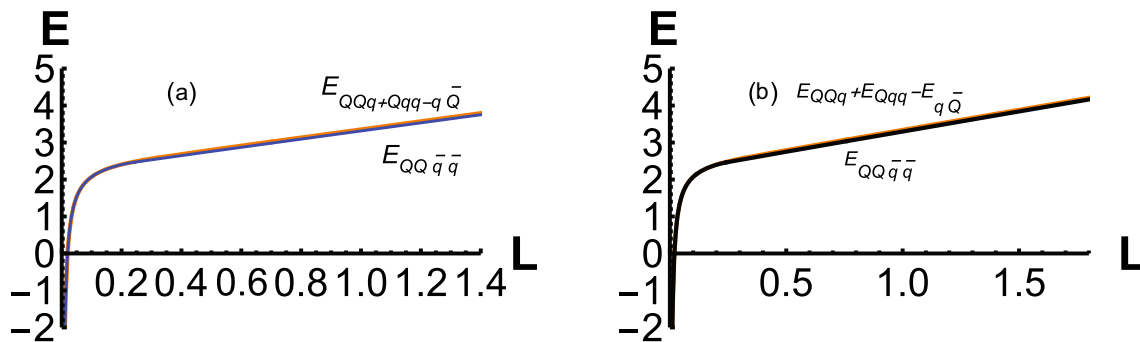


Fig. 19 a The energy of $QQ\bar{q}\bar{q}$ and $QQq + Qqq - q\bar{q}$ at $T = 0$ GeV. b The energy of $QQ\bar{q}\bar{q}$ and $QQq + Qqq - q\bar{q}$ at $T = 0.08$ GeV

China (Grant No. 21B0402), and the National Natural Science Foundation of China Grants under No. 12175100.

Data availability This manuscript has no associated data or the data will not be deposited. [Authors' comment: This is a theoretical study and no experimental data.]

Open Access This article is licensed under a Creative Commons Attribution 4.0 International License, which permits use, sharing, adaptation, distribution and reproduction in any medium or format, as long as you give appropriate credit to the original author(s) and the source, provide a link to the Creative Commons licence, and indicate if changes were made. The images or other third party material in this article are included in the article's Creative Commons licence, unless indicated otherwise in a credit line to the material. If material is not

included in the article's Creative Commons licence and your intended use is not permitted by statutory regulation or exceeds the permitted use, you will need to obtain permission directly from the copyright holder. To view a copy of this licence, visit <http://creativecommons.org/licenses/by/4.0/>. Funded by SCOAP³.

References

1. J.M. Maldacena, The Large N limit of superconformal field theories and supergravity. *AIP Conf. Proc.* **484**(1), 51 (1999)

2. O. Aharony, S.S. Gubser, J.M. Maldacena, H. Ooguri, Y. Oz, Large N field theories, string theory and gravity. *Phys. Rep.* **323**, 183–386 (2000)
3. J.M. Maldacena, Wilson loops in large N field theories. *Phys. Rev. Lett.* **80**, 4859–4862 (1998)
4. O. Andreev, Baryon modes in string breaking from gauge/string duality. *Phys. Lett. B* **804**, 135406 (2020)
5. S.-J. Rey, S. Theisen, J.-T. Yee, Wilson–Polyakov loop at finite temperature in large N gauge theory and anti-de Sitter supergravity. *Nucl. Phys. B* **527**, 171–186 (1998)
6. A. Brandhuber, N. Itzhaki, J. Sonnenschein, S. Yankielowicz, Wilson loops in the large N limit at finite temperature. *Phys. Lett. B* **434**, 36–40 (1998)
7. J. Casalderrey-Solana, H. Liu, D. Mateos, K. Rajagopal, U.A. Wiedemann, *Gauge/String Duality, Hot QCD and Heavy Ion Collisions* (Cambridge University Press, Cambridge, 2014)
8. Z. Zhang, D. Hou, G. Chen, Heavy quark potential from deformed AdS_5 models. *Nucl. Phys. A* **960**, 1–10 (2017)
9. O. Andreev, V.I. Zakharov, Heavy-quark potentials and AdS/QCD. *Phys. Rev. D* **74**, 025023 (2006)
10. K.B. Fadafan, Heavy quarks in the presence of higher derivative corrections from AdS/CFT. *Eur. Phys. J. C* **71**, 1799 (2011)
11. O. DeWolfe, S.S. Gubser, C. Rosen, A holographic critical point. *Phys. Rev. D* **83**, 086005 (2011)
12. X. Chen, L. Zhang, D. Hou, Running coupling constant at finite chemical potential and magnetic field from holography *. *Chin. Phys. C* **46**(7), 073101 (2022)
13. J. Zhou, X. Chen, Y.-Q. Zhao, J. Ping, Thermodynamics of heavy quarkonium in a magnetic field background. *Phys. Rev. D* **102**(8), 086020 (2020)
14. X. Chen, D. Li, D. Hou, M. Huang, Quarkyonic phase from quenched dynamical holographic QCD model. *JHEP* **03**, 073 (2020)
15. H. Bohra, D. Dudal, A. Hajilou, S. Mahapatra, Anisotropic string tensions and inversely magnetic catalyzed deconfinement from a dynamical AdS/QCD model. *Phys. Lett. B* **801**, 135184 (2020)
16. T. Alho, M. Järvinen, K. Kajantie, E. Kiritsis, C. Rosen, K. Tuominen, A holographic model for QCD in the Veneziano limit at finite temperature and density. *JHEP* **04**, 124 (2014) [Erratum: *JHEP* **02**, 033 (2015)]
17. X. Chen, L. Zhang, D. Li, D. Hou, M. Huang, Gluodynamics and deconfinement phase transition under rotation from holography. *JHEP* **07**, 132 (2021)
18. J. Erlich, E. Katz, D.T. Son, M.A. Stephanov, QCD and a holographic model of hadrons. *Phys. Rev. Lett.* **95**, 261602 (2005)
19. X. Chen, D. Li, M. Huang, Criticality of QCD in a holographic QCD model with critical end point. *Chin. Phys. C* **43**(2), 023105 (2019)
20. I. Aref’eva, K. Rannu, Holographic anisotropic background with confinement-deconfinement phase transition. *JHEP* **05**, 206 (2018)
21. C. Ewerz, O. Kaczmarek, A. Samberg, Free energy of a heavy quark-antiquark pair in a thermal medium from AdS/CFT. *JHEP* **03**, 088 (2018)
22. J. Casalderrey-Solana, H. Liu, D. Mateos, K. Rajagopal, U.A. Wiedemann, *Gauge/String Duality, Hot QCD and Heavy Ion Collisions* (Cambridge University Press, Cambridge, 2014)
23. Z. Fang, S. He, D. Li, Chiral and deconfining phase transitions from holographic QCD study. *Nucl. Phys. B* **907**, 187–207 (2016)
24. H.-T. Ding, F. Karsch, S. Mukherjee, Thermodynamics of strong-interaction matter from Lattice QCD. *Int. J. Mod. Phys. E* **24**(10), 1530007 (2015)
25. J. Zhou, X. Chen, Y.-Q. Zhao, J. Ping, Thermodynamics of heavy quarkonium in rotating matter from holography. *Phys. Rev. D* **102**(12), 126029 (2021)
26. R.-G. Cai, S. He, D. Li, A hQCD model and its phase diagram in Einstein–Maxwell–Dilaton system. *JHEP* **03**, 033 (2012)
27. D. Li, S. He, M. Huang, Q.-S. Yan, Thermodynamics of deformed AdS_5 model with a positive/negative quadratic correction in graviton-dilaton system. *JHEP* **09**, 041 (2011)
28. D. Li, M. Huang, Q.-S. Yan, A dynamical soft-wall holographic QCD model for chiral symmetry breaking and linear confinement. *Eur. Phys. J. C* **73**, 2615 (2013)
29. J.-M. Richard, A. Valcarce, J. Vijande, Doubly-heavy baryons, tetraquarks, and related topics. *Bled Workshops Phys.* **19**, 24 (2018)
30. R. Aaij et al., Observation of an exotic narrow doubly charmed tetraquark. *Nat. Phys.* **18**(7), 751–754 (2022)
31. I.T. Drummond, Strong coupling model for string breaking on the lattice. *Phys. Lett. B* **434**, 92–98 (1998)
32. J. Sonnenschein, D. Weissman, A tetraquark or not a tetraquark? A holography inspired stringy hadron (HISH) perspective. *Nucl. Phys. B* **920**, 319–344 (2017)
33. O. Andreev, Some multi-quark potentials, pseudo-potentials and AdS/QCD. *Phys. Rev. D* **78**, 065007 (2008)
34. J. Najjar, G. Bali, Static-static-light baryonic potentials. *PoS, LAT2009:089* (2009)
35. A. Yamamoto, H. Suganuma, H. Iida, Lattice QCD study of the heavy-heavy-light quark potential. *Phys. Rev. D* **78**, 014513 (2008)
36. A. Francis, R.J. Hudspith, R. Lewis, K. Maltman, More on heavy tetraquarks in lattice QCD at almost physical pion mass. *EPJ Web Conf.* **175**, 05023 (2018)
37. O. Andreev, QQq potential in string models. *Phys. Rev. D* **105**(8), 086025 (2022)
38. O. Andreev, Model of the N -quark potential in $SU(N)$ gauge theory using gauge-string duality. *Phys. Lett. B* **756**, 6–9 (2016)
39. J. Bulava, B. Hörz, F. Knechtli, V. Koch, G. Moir, C. Morningstar, M. Peardon, String breaking by light and strange quarks in QCD. *Phys. Lett. B* **793**, 493–498 (2019)
40. Y. Li, C.W. von Keyserlingk, G. Zhu, T. Jochym-O’Connor, Phase diagram of the three-dimensional subsystem toric code. *5* (2023)
41. Y. Yang, P.-H. Yuan, Confinement-deconfinement phase transition for heavy quarks in a soft wall holographic QCD model. *JHEP* **12**, 161 (2015)
42. X. Chen, S.-Q. Feng, Y.-F. Shi, Y. Zhong, Moving heavy quarkonium entropy, effective string tension, and the QCD phase diagram. *Phys. Rev. D* **97**(6), 066015 (2018)
43. X. Chen, D. Li, D. Hou, M. Huang, Quarkyonic phase from quenched dynamical holographic QCD model. *JHEP* **03**, 073 (2020)
44. J. Zhou, X. Chen, Y.-Q. Zhao, J. Ping, Thermodynamics of heavy quarkonium in a magnetic field background. *Phys. Rev. D* **102**(8), 086020 (2020)
45. O. Andreev, V.I. Zakharov, On heavy-quark free energies, entropies, Polyakov loop, and AdS/QCD. *JHEP* **04**, 100 (2007)
46. O. Andreev, V.I. Zakharov, The spatial string tension, thermal phase transition, and AdS/QCD. *Phys. Lett. B* **645**, 437–441 (2007)
47. S. He, M. Huang, Q. Yan, Heavy quark potential and QCD beta function from a deformed AdS_5 model. *Prog. Theor. Phys. Suppl.* **186**, 504–509 (2010)
48. O. Andreev, Some properties of the QQq -quark potential in string models. *JHEP* **05**, 173 (2021)
49. X. Chen, Yu. Bo, P.-C. Chu, X. Li, Studying the potential of QQq at finite temperature in a holographic model *. *Chin. Phys. C* **46**(7), 073102 (2022)
50. O. Andreev, Some thermodynamic aspects of pure glue, fuzzy bags and gauge/string duality. *Phys. Rev. D* **76**, 087702 (2007)
51. E. Witten, Baryons and branes in anti-de Sitter space. *JHEP* **07**, 006 (1998)
52. E. Witten, Anti-de Sitter space and holography. *Adv. Theor. Math. Phys.* **2**, 253–291 (1998)
53. O. Aharony, E. Witten, Anti-de Sitter space and the center of the gauge group. *JHEP* **11**, 018 (1998)

54. O. Andreev, String breaking, baryons, medium, and gauge/string duality. *Phys. Rev. D* **101**(10), 106003 (2020)
55. O. Andreev, Some aspects of three-quark potentials. *Phys. Rev. D* **93**(10), 105014 (2016)
56. O. Andreev, Remarks on static three-quark potentials, string breaking and gauge/string duality. *Phys. Rev. D* **104**(2), 026005 (2021)
57. K. Peeters, J. Sonnenschein, M. Zamaklar, Holographic melting and related properties of mesons in a quark gluon plasma. *Phys. Rev. D* **74**, 106008 (2006)
58. C. Hoyos-Badajoz, K. Landsteiner, S. Montero, Holographic meson melting. *JHEP* **04**, 031 (2007)
59. K. Bitaghsir Fadafan, E. Azimfard, On meson melting in the quark medium. *Nucl. Phys. B* **863**, 347–360 (2012)
60. C.D. White, The Cornell potential from general geometries in AdS/QCD. *Phys. Lett. B* **652**, 79–85 (2007)
61. V.N. Gribov, Quantization of nonabelian gauge theories. *Nucl. Phys. B* **139**, 1 (1978)
62. A. Karch, E. Katz, D.T. Son, M.A. Stephanov, Linear confinement and AdS/QCD. *Phys. Rev. D* **74**, 015005 (2006)
63. A. Bazavov et al., The chiral and deconfinement aspects of the QCD transition. *Phys. Rev. D* **85**, 054503 (2012)